chemosensors

MDPI

Article

2,12-Diaza[6]helicene: An Efficient Non-Conventional Stereogenic Scaffold for Enantioselective Electrochemical Interphases

Francesca Fontana [1,*], Benedetta Bertolotti [1], Sara Grecchi [2], Patrizia Romana Mussini [2], Laura Micheli [3], Roberto Cirilli [4], Matteo Tommasini [5] and Simona Rizzo [6,*]

1 Dipartimento di Ingegneria e Scienze Applicate, Università di Bergamo, 24044 Dalmine, Italy; benedetta.bertolotti@unibg.it
2 Dipartimento di Chimica, Università Degli Studi di Milano, Via Golgi 19, 20133 Milano, Italy; sara.grecchi@unimi.it (S.G.); patrizia.mussini@unimi.it (P.R.M.)
3 Dipartimento di Scienze e Tecnologie Chimiche, Università Degli Studi di Roma Tor Vergata, Via della Ricerca Scientifica 1, 00133 Rome, Italy; laura.micheli@uniroma2.it
4 Centro Nazionale per Il Controllo e la Valutazione dei Farmaci, Istituto Superiore di Sanità, Viale Regina Elena 299, 00161 Rome, Italy; roberto.cirilli@iss.it
5 Dipartimento di Chimica, Materiali e Ing. Chimica "G. Natta", Politecnico di Milano, Piazza Leonardo da Vinci 32, 20133 Mlano, Italy; matteo.tommasini@polimi.it
6 CNR Istituto di Scienze e Tecnologie Chimiche "Giulio Natta", Via C. Golgi 19, 20133 Milano, Italy
* Correspondence: francesca.fontana@unibg.it (F.F.); simona.rizzo@scitec.cnr.it (S.R.)

Abstract: The new configurationally stable, unsymmetrical 2,12-diaza[6]helicene was synthesized as a racemate and the enantiomers were separated in an enantiopure state by semi-preparative HPLC on chiral stationary phase. Under selected alkylation conditions it was possible to obtain both the enantiopure 2-*N*-mono- and di-*N*-ethyl quaternary iodides. Metathesis with bis(trifluoromethanesulfonyl)imide anion gave low-melting salts which were tested as inherently chiral additives to achiral ionic liquids for the electrochemical enantiodiscrimination of chiral organic probes in voltammetric experiments. Remarkable differences in the oxidation potentials of the enantiomers of two probes, a chiral ferrocenyl amine and an aminoacid, were achieved; the differences increase with increasing additive concentration and number of alkylated nitrogen atoms.

Keywords: azahelicenes; chiral voltammetry; enantiodiscrimination; ionic liquids; chiral additives

check for updates

Citation: Fontana, F.; Bertolotti, B.; Grecchi, S.; Mussini, P.R.; Micheli, L.; Cirilli, R.; Tommasini, M.; Rizzo, S. 2,12-Diaza[6]helicene: An Efficient Non-Conventional Stereogenic Scaffold for Enantioselective Electrochemical Interphases. *Chemosensors* **2021**, *9*, 216. https://doi.org/10.3390/chemosensors9080216

Academic Editors: Victor Borovkov, Riina Aav, Roberto Paolesse, Manuela Stefanelli and Donato Monti

Received: 30 June 2021
Accepted: 4 August 2021
Published: 10 August 2021

Publisher's Note: MDPI stays neutral with regard to jurisdictional claims in published maps and institutional affiliations.

Copyright: © 2021 by the authors. Licensee MDPI, Basel, Switzerland. This article is an open access article distributed under the terms and conditions of the Creative Commons Attribution (CC BY) license (https://creativecommons.org/licenses/by/4.0/).

1. Introduction

We have recently developed a research in the field of chiral ionic liquids (CILs), and more broadly organic ammonium salts, with the aim of designing new sensing materials endowed with powerful discrimination ability for enantiomeric pairs of different nature, functionalization and use. In particular, we investigated the effects of the structural relationships between the group constituting the stereogenic element responsible for chirality and the ammonium function characterizing the properties: we demonstrated that the coincidence of these moieties, which occurs in Inherently Chiral (IC) materials, strongly enhances the enantiodiscrimination ability of a CIL [1,2] while the structural independence of these units, which corresponds to the most popular design of CILs, is followed by more modest enantioselection results [3].

In particular, we demonstrated that IC enantiopure bi-benzimidazolium salts (**1**) [1] and bicollidinium (**2**) [2] (Figure 1), when used as additives to achiral ILs, produce remarkable differences (up to 360 mV) in the oxidation potentials of the enantiomers of different probes (ferrocenyl-ethylamine [1,2], DOPA methyl ester [2], inherently chiral thiophene based monomer BT_2T_4 [2]) in CV experiments.

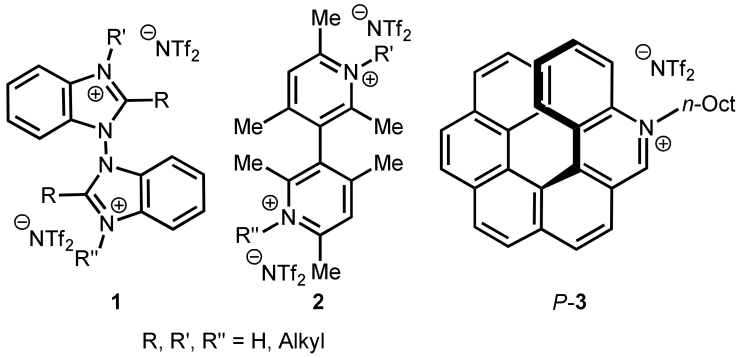

Figure 1. bi-benzimidazolium (**1**), bicollidinium (**2**) and (*P*)-aza[6]helicenium bistriflimidate (**3**) salts.

We recently extended our investigation from IC salts **1** and **2**, characterized by a stereogenic axis, to IC helical compounds. We synthesized the 5-octyl-5-aza[6]helicenium bistriflimidate (**3**), prompted by the consideration that aza[*n*]helicenes are a class of chiral molecules possessing peculiar electronic and chiroptical properties [4] and display high configurational stability when constituted by at least six fused 6-membered rings [5]. Furthermore, these salts exhibited very good enantiodiscrimination ability for the antipodes of benchmark ferrocenyl ethyl amine as well as tyrosine methyl ester [6].

The investigations carried out on (**1**) clearly demonstrated a remarkably progressive stereoselectivity enhancement from plain bicollidine to the corresponding mono-alkylated compounds and then to the di-alkylated salts [1].

The aim of the present work was to check the possibility of increasing the enantioselection ability of the aza-helicenium compound (**3**) by introducing a further quaternary ammonium function on the helical scaffold. In this light, the synthesis of the enantiomerically pure antipodes of new 2,12-diaza[6]helicene (4) was planned (Figure 2).

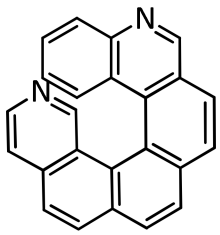

Figure 2. 2,12-diaza[6]helicene (**4**).

Mono- and dialkylation could afford a platform of salts to be tested as chirality inducers for achiral ILs in chiral voltammetry experiments, according to a well-established paradigm. The investigation could also give a further proof of the parallel increase of enantiorecognition ability vs. the number of quaternarized nitrogen atoms.

2. Materials and Methods

The starting materials and solvents for azahelicene synthesis were purchased from Carlo Erba (Milan, Italy) and used without further purification; photolysis reactions were performed on a Multirays instrument (Helios Italquartz, Cambiago, Italy) equipped with sets of 10 lamps of different wavelength; NMR spectra were recorded on Bruker AV400 and Bruker AV300 spectrometers. Chemical shifts (δ) are expressed in parts per million (ppm), and coupling constants are given in Hz. Splitting patterns are indicated as follows: s = singlet, d = doublet, t = triplet, q = quartet, m = multiplet. Purifications by column chromatography were performed using Merck silica gel 60 (230–400 mesh for flash-chromatography and 70–230 mesh for gravimetric chromatography) and aluminium oxide 90 neutral. GC-MS analyses were performed on an Agilent 6850 chromatograph

equipped with an Agilent 5975N mass spectrometer. UV-Vis spectra were measured with a Jasco V-650 spectrometer. LC-MS analyses were performed with direct infusion of the sample (ACN/H_2O solvent carrier) on a Shimadzu LCMS2020 ESI/DUIS mass detector.

HPLC-grade solvents were purchased from Sigma-Aldrich (Milan, Italy). HPLC enantioseparations were performed by using stainless-steel Chiralpak IA (250 mm × 4.6 mm, 5 µm and 250 mm × 10 mm, 5 µm) columns (Chiral Technologies Europe, Illkirch, France). The HPLC apparatus used for analytical enantioseparations consisted of a Perkin Elmer (Norwalk, CT, USA) 200 LC pump equipped with a Rheodyne (Cotati, CA, USA) injector, a 50 µL sample loop, an HPLC PerkinElmer oven and a Jasco (Jasco, Tokyo, Japan) Model CD2095 Plus UV/CD detector. The signal was acquired and processed by Clarity software (DataApex, Prague, Czech Republic). For semi-preparative separation, a PerkinElmer 200 LC pump equipped with a Rheodyne injector, a 5000 µL sample loop, a PerkinElmer LC 101 oven and Waters 484 detector (Waters Corporation, Milford, MA, USA) were used.

The CD spectra of the enantiomers collected on a semipreparative scale were recorded in dichloromethane at 25 °C by using a Jasco Model J-700 spectropolarimeter. The optical path was 0.1 cm. The spectra are average computed over two instrumental scans and the intensities are presented in terms of ellipticity values (mdeg).

The quantum chemical calculations have been carried out with the Gaussian software [7] adopting the B3LYP functional and the 6–31G(d,p) basis set. Electrostatic atomic charges have been evaluated by the Hirshfeld method [8].

3. Results and Discussion

3.1. Synthesis of 2,12-Diaza[6]helicene

The synthesis of (±)-**4** (Scheme 1) was at first attempted through a classical Wittig approach, as in [6], starting from a condensation between quinoline-3-carboxaldehyde and 4-methyl benzylphosphonium bromide, to obtain stilbene intermediate (**5**), which is then photochemically cyclized by irradiation with 366 nm lamp.

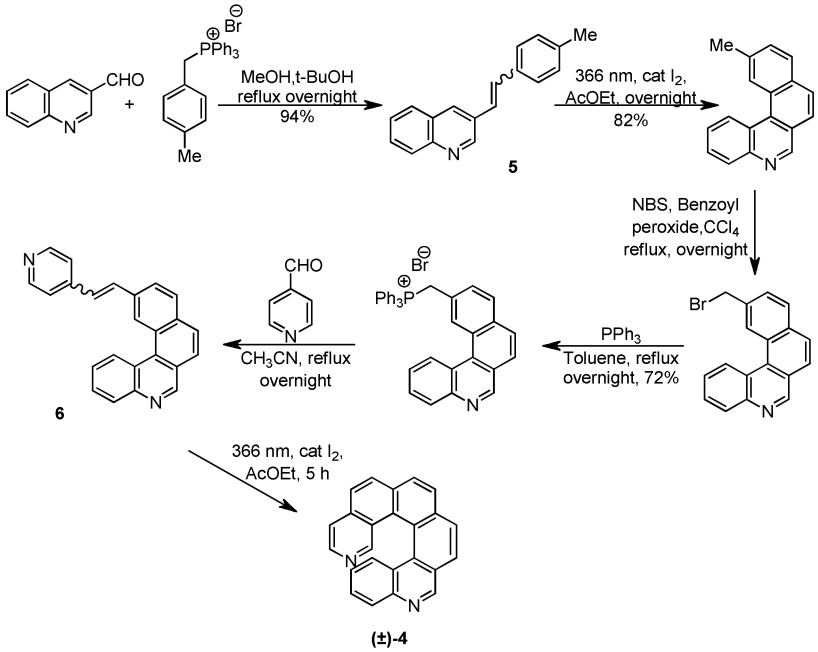

Scheme 1. diaza[6]helicene ((±)-**4**).

The methyl group is then brominated with NBS and converted into the corresponding phosphonium salt. A second Wittig condensation with pyridine-4-carboxaldehyde yielded intermediate (**6**) which, upon photochemical cyclization at 366 nm, formed compound (**4**).

The problem we encountered at this point concerned the purification of the product, since it proved very difficult to eliminate Ph_3PO by column chromatography, either on

silica gel or alumina. The reaction product and Ph_3PO display quite similar polarity and affinity with the stationary phase and we could not obtain pure fractions. Therefore we tried to remove Ph_3PO by complexing it with $ZnCl_2$ [9]. By doing so, we realized that compound (**4**) tends itself to form complexes with Zn^{2+} ions, so that this purification method was not viable. We then decided to modify our synthetic strategy by substituting the second Wittig condensation with a Heck reaction, as indicated in Scheme 2.

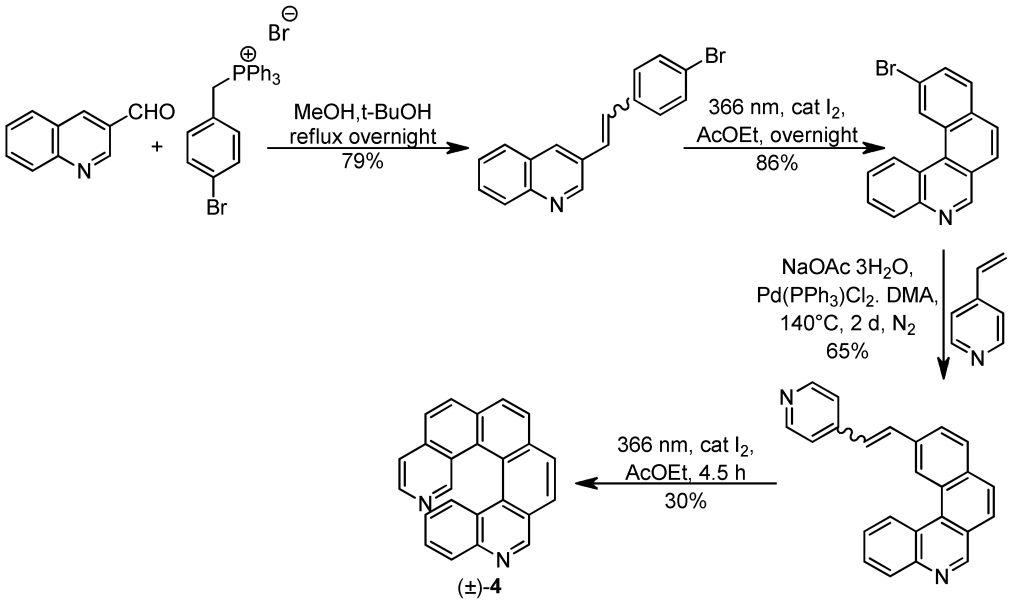

Scheme 2. Alternative synthesis for (±)-**4**.

In this case we obtained product **4** in 30% yield, without encountering particular problems in purification. Its structure is supported by analytical and spectral data (^{1}H and APT NMR, COSY, NOESY, HSQC, HMBC experiments, MS and UV; see Supplementary Materials).

3.2. Resolution of the Enantiomers

The direct resolution of (±)-**4** was successfully carried out by HPLC on the polysaccharide-based Chiralpak IA chiral stationary phase (CSP). Optimized chromatographic conditions were achieved by using the mixture *n*-hexane-acetone-2-propanol-diethylamine 50:50:0.2:0.2 (*v*/*v*/*v*/*v*) as a mobile phase and setting the column temperature at 5 °C (Figure 3a). The use of the immobilized-type Chiralpak IA CSP in combination with a mobile phase containing a non-standard solvent such as acetone allowed a good chiral recognition in terms of enantioselectivity and resolution degree. Furthermore, this condition was extremely attractive for mg-scale enantioseparations due to the high solvating power of acetone and the relative simplicity of the evaporation of the mobile phase. The analytical separations were easily scaled up to the milligram range using a 250 mm × 10 mm Chiralpak IA column (Figure 3b). Iterative chromatography of 3.3 mg of racemic sample, followed by fraction collection and pooling, allowed to collect multimilligram quantities of individual enantiomers with ee >99.9%. The assignment of the absolute configuration of **4** was carried out by comparing the circular dichroism (CD) properties of the enantiomers isolated on a semipreparative scale with those of the enantiomers of the structurally related 5-aza-[6]-helicene, whose stereochemistry was established in a previous work [10]. The first eluted enantiomer exhibited a clear bisegnate CD spectrum in the 450−220 nm spectral range with a maximum and a minimum of ellipticity located at 324 and 243 nm, respectively. As shown in Figure 4, the CD profile of the less eluted enantiomer of **4** was in strict agreement, both in sign and magnitude, with the CD spectrum of the (*P*)-enantiomer

of the parent helicene. Furthermore, as expected, the shape of the CD spectrum of the second eluted enantiomer (*M*)-**4** was perfectly specular to that of the (*P*)-enantiomer.

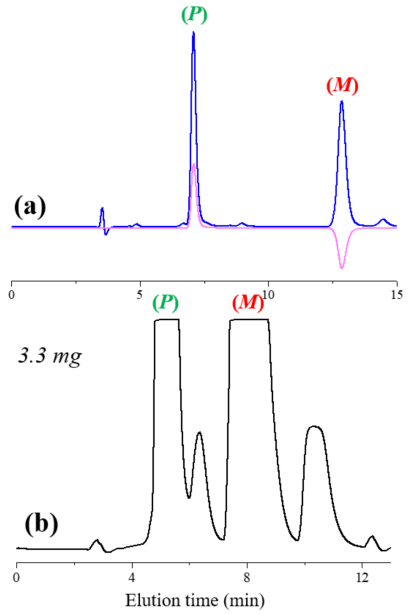

Figure 3. Typical chromatograms illustrating the (**a**) analytical and (**b**) semipreparative enantioseparation of **4**. Detector, UV/CD at 330 nm (**a**) and UV at 330 nm (**b**).

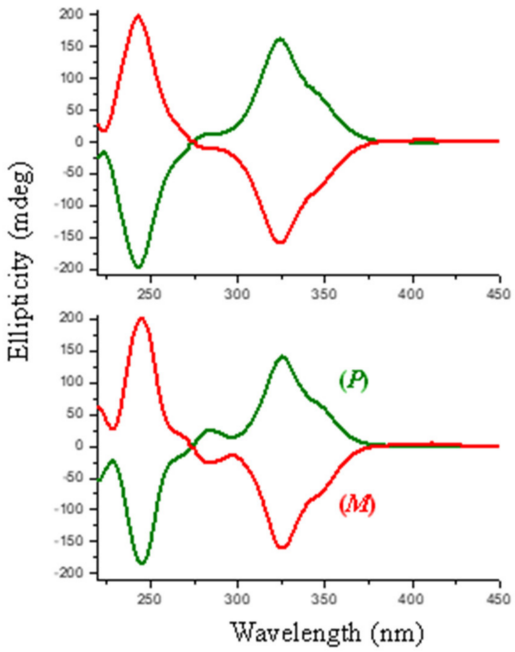

Figure 4. CD spectra of the enantiomers of **4** (top) and 5-aza-[6]-helicene (bottom) in dichloromethane.

*3.3. Alkylation of (P)-**4** and (M)-**4***

As one of the nitrogen atoms in the helical framework reacts with an alkylating reagent, the positive charge developed on it exerts a strong inductive effect over the second one, whose nucleophicility is consequently reduced [11]. Thus, the second alkylation to give the doubly quaternarized derivative is more difficult than the first one and requires harsher experimental conditions. The consequence is that it is possible to selectively accede to both mono- and di-substituted salts. However, since the two nitrogen atoms are constitutionally heterotopic, the question arises about which one would be alkylated first.

By dissolving enantiopure compounds (*P*)-**4**/(*M*)-**4** in neat ethyl iodide and stirring the mixture at r.t. for 2.5 days, the insoluble mono-alkylated salts (*P*)-**7** and (*M*)-**7** were obtained by simple filtration (vide infra). These, upon heating with ethyl iodide at 50 °C for 11 days, and then for 2.5 days after acetonitrile addition, afforded the doubly quaternarized derivatives (*P*)-**8** and (*M*)-**8**, respectively (Figure 5).

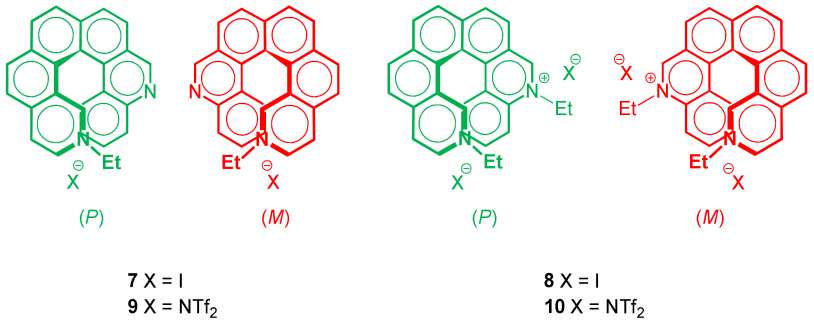

Figure 5. *N*-ethyl-2,12-diaza[6]helicene-2-ium (**7**,**9**) and *N*,*N*′-diethyl-2,12-diaza[6]helicene-2,12-diium (**8**,**10**) salts.

Iodide counteranion was then exchanged with bis (trifluoromethanesulfonyl)imidate (bis-triflimidate, NTf_2), since it would not be stable during electrochemical experiments, Both mono-ethyl-bistriflimidates (*P*)-**9** and (*M*)-**9** and diethyl-bistriflimidates (*P*)-**10** and (*M*)-**10** enantiopure quaternary salts have been obtained as yellow waxy solids (Figure 5).

Despite the expected higher steric hindrance we found that the nitrogen atom in position 2 is the first to react with ethyl iodide to give the 2-(N-ethyl)-2,12-diaza[6]helicenium iodides (*P*)-**7** and (*M*)-**7**. This assignment is based on spectroscopic experiments (^{1}H NMR, COSY, NOESY, ^{13}C NMR, HSQC, HMBC; see Supplementary Materials). In particular the signals of the hydrogen atoms of **4** located in position 3 and 4 undergo a remarkable shift towards lower fields in **7,** due to the electronic availability decrease on the neighbouring nitrogen atom (Figure 6). Further proof is given by NOESY experiments of **7**, which revealed the cross peaks between the methylenic hydrogens of the ethyl group and the hydrogens in positions 1 and 3 (Figure 7).

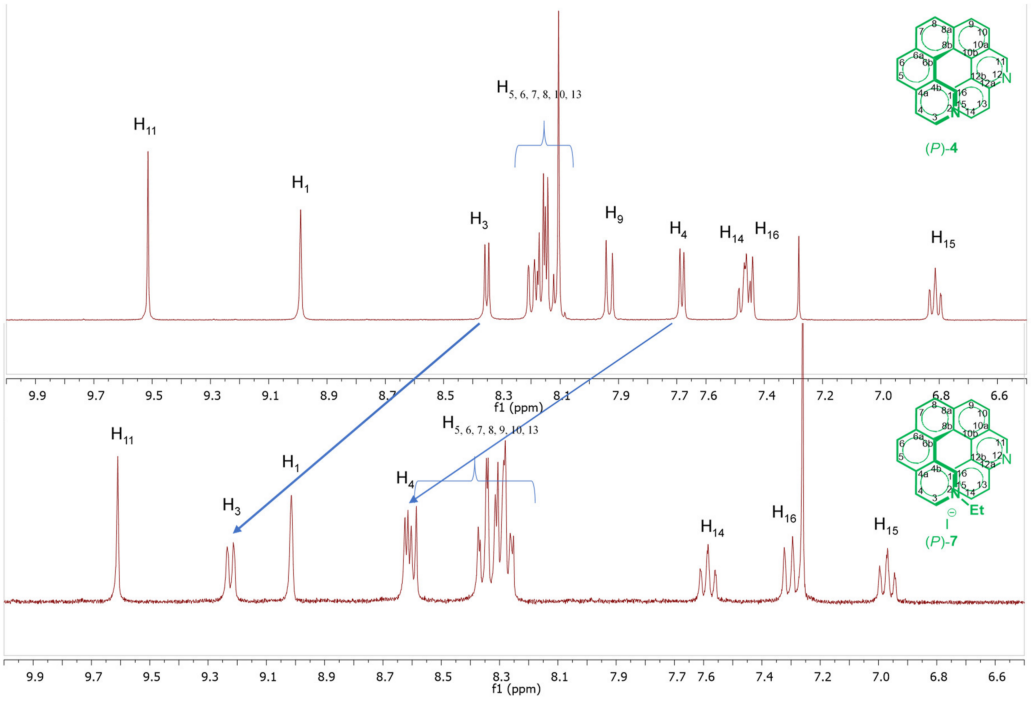

Figure 6. Comparison of ^{1}H-NMR spectra of **4** and **7**.

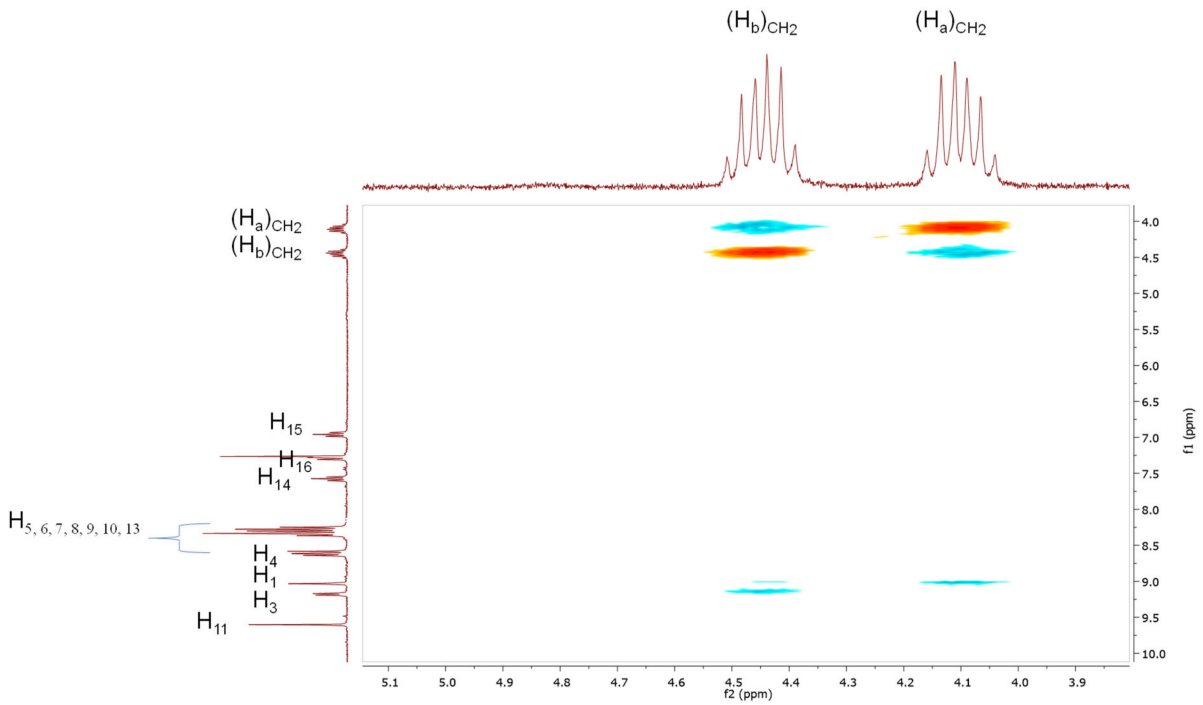

Figure 7. NOESY experiment on **7**.

To rationalize the different chemical behaviour of the two nitrogen atoms we have also carried out a series of DFT calculations to ascertain the atomic charge of the two nitrogen atoms. We report in Table 1 the electrostatic Hirshfeld charges [8] computed with two popular DFT functionals (B3LYP, M06–2X) and basis sets, namely the compact 6–31G(d,p) and the more accurate jun-cc-pVTZ. It is evident that the two nitrogens of **4** essentially display the same electrostatic charge, irrespective of the DFT functional and basis set. All the selected computational setups agree on the fact that the charge on N(2) is slightly more negative (by just 0.002 atomic units) than the charge on N(12). This minor difference is not enough to justify a marked preference of N(2) or N(12) to alkylation.

Table 1. DFT-computed energies (hartree units) and Hirshfeld charges (atomic units) of the two nitrogen atoms of **4**.

	B3LYP/6–31g(d,p)	**B3LYP/Jun-cc-pVTZ**	**M06–2X/6–31g(d,p)**	**M06–2X/Jun-cc-pVTZ**
Energy (ha)	−1032.54128065	−1032.85778413	−1032.12555221	−1032.46026159
Q[N(2)]	−0.196	−0.190	−0.194	−0.190
Q[N(12)]	−0.194	−0.188	−0.192	−0.188
Q[N(2)] − Q[N(12)]	−0.002	−0.002	−0.002	−0.002

Therefore, we have also computed the relative energetic stability of the two alkylated derivatives of **4**. For the sake of simplicity, we limit ourselves to the results obtained with the extended basis set (jun-cc-pVTZ). Clearly, given that the alkylation reaction has fixed reactants (**4** and ethyl iodide) a significantly lower energy of the product alkylated at N(2) or N(12) may suggest a preference for the first alkylation occurring at a specific site.

As reported in Table 2, the B3LYP and the M06–2X functionals agree on the energy difference between the two alkylated products, that is limited to just a few kcal/mol. Such energy difference is not due to a difference in the electron density of the two nitrogen atoms (see Table 1), hence we expect that it should be due to differences in the intramolecular interactions between the alkyl substituent and the helicene moiety. This is supported by the inspection of the relative position of the CH bonds of the ethyl group vs. the vicinal

helicene (see Figure 8). Therefore, the observed occurrence of a preference for the first alkylation at N(2) should be mainly due to steric effects rather than differences in the electron density at the nitrogen sites.

Table 2. DFT-computed energies (hartree units) and relative stabilities (kcal/mol) of the ethylated derivatives of **4**. The labels of the isomers correspond to the structures reported in Figure 8.

B3LYP/jun-cc-pVTZ		
ID and Ethylation Site	**Energy (ha)**	**ΔE (kcal/mol)**
A—N(2)	−1111.90878265	0.0
A′—N(2)	−1111.90864474	0.1
B—N(12)	−1111.90386408	3.1
M06–2X/jun-cc-pVTZ		
ID and Ethylation Site	**Energy (ha)**	**ΔE (kcal/mol)**
A—N(2)	−1111.46570147	0.8
A′—N(2)	−1111.46703268	0.0
B—N(12)	−1111.46068086	4.0

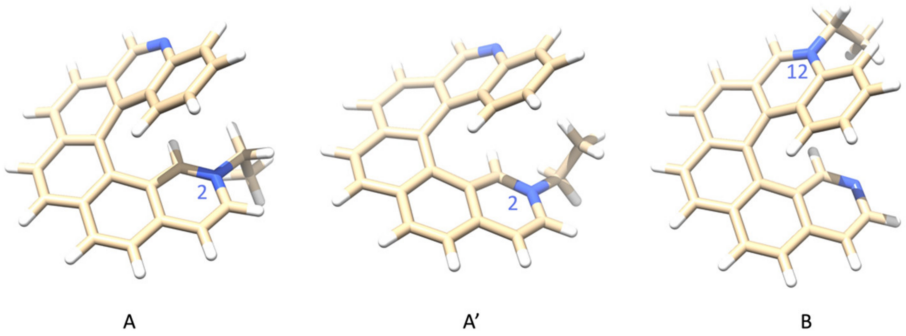

Figure 8. Equilibrium structures of 2-(*N*-ethyl)-2,12-diaza[6]helicenium (**A**,**A′**) and 12-(*N*-ethyl)-2,12-diaza[6]helicenium (**B**) computed by the M06–2X/jun-cc-pVTZ DFT method (singlet cations). The representation of the structures of same isomers obtained by B3LYP/jun-cc-pVTZ calculations is very similar.

3.4. Electrochemical Characterization

Cyclic voltammetry experiments were performed on compound (**4**) on a glassy carbon GC electrode. Positive and negative half cycles have been separately recorded to avoid reciprocal contamination by electron transfer products. The reported potentials have been normalized vs the formal potential of the intersolvental ferricinium | ferrocene (Fc^+ | Fc) reference redox couple, recorded in the same conditions, whereas currents are normalized against surface, concentration and square root of scan rate, assuming the diffusive character of the electron transfer processes.

A synopsis of the normalized CV patterns of **4**, **9** and **10** is provided in Figure 9, and the corresponding CV peak potentials are collected in Table 3 and compared with those formerly observed for two monoazahelicene compounds, i.e., 5-aza[6]helicene and its *N*-octyl-5-aza[6]helicenium bistriflimidate salt [6].

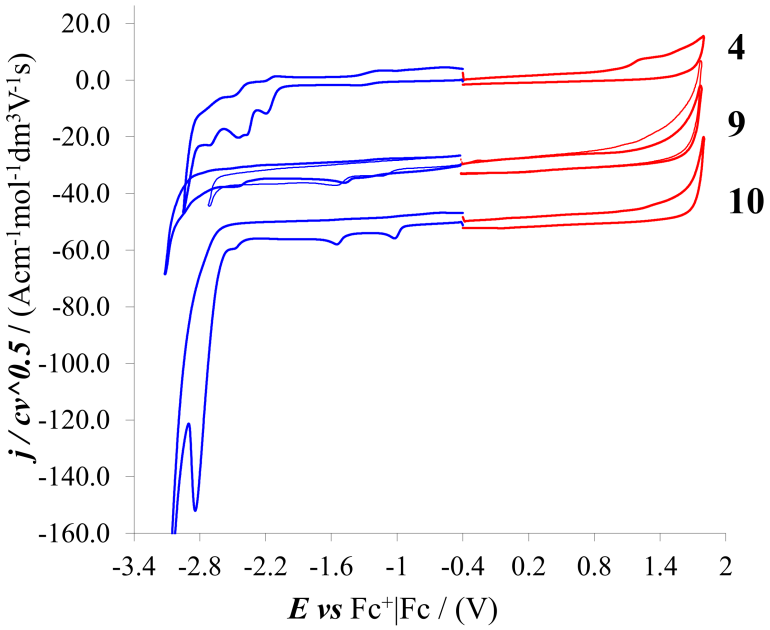

Figure 9. CV patterns for compound **4** and for the bis-triflimidates **9** and **10**, 0.00075 M solutions in ACN + 0.1 M $TBAPF_6$ on GC electrode at 0.2 V/s scan rate.

Table 3. CV peak potentials, normalized vs the Fc^+ | Fc couple, for oxidative and reductive electron transfer processes of diazahelicene compounds **4**, **9** and **10** and of two monoazahelicene compounds [6], for comparison.

	$E_{p,\,Ia}$/V	$E_{p,\,Ic}$/V
5-aza[6]helicene [6]	1.07, 1.47	−2.25, −2.52, −2.66
N-octyl-5-aza[6]helicenium bistriflimidate [6]	1.46	−1.19 (nearly splitting), −2.58
4	1.26	−2.16, 2.41,−2.48, −2.73
9	no peaks	−1.52 (with prepeak); −2.47
10	no peaks	−1.00, −1.52, −2.45, −2.83

By comparing the parent diazahelicene with its mono- and di-alkylated salts, the most evident feature is the inversion in redox activity already observed in the mono case [6], since conversion of the nitrogen sites into alkylated cations turns them from electron rich to electron poor. In particular:

(i) *only diazahelicene undergoes oxidation within the available electrochemical window*. Only one irreversible oxidation peak, followed by a shoulder, is perceivable before the background. It should correspond to oxidation of one of the nitrogen sites, according to the similar value measured for monoazahelicene [6] and significantly less positive than that of carbahelicenes. Given the above-mentioned conjugation between nitrogen sites, the second oxidation should take place at more positive potentials.

Instead, no oxidation peak at all is observed either for **10**, in which both N positions are alkylated, and for **9**, featuring a free N position besides an alkylated one. This observation might be justified by considering the above-mentioned conjugation between the two nitrogen sites, which reduces the electron density on both of them compared to the parent diazahelicene **4**.

(ii) *huge positive shift of reduction peak potentials with strong reciprocal interaction between N sites for cations:* Parent diazahelicene **4** features a complex reduction peak system, although starting with a monoelectronic chemically and electrochemically reversible peak. This can be assumed to account for reductions on both helicene sides, in the

−2.2/−2.8 V range, similar to that formerly observed for the monoazahelicene case. There are, however, differences in peak potentials and multiplicity, consistently with the change in the nature of the two terminals. Instead in the case of **9** a reduction peak is observed at −1.52 V, i.e., much more positive respect to **4**, as the nitrogen site, becoming cationic, now provides a preferential site for the first reduction. However, such potential is significantly less positive than the one observed in the case of the monoaza analogue. Since in monoazahelicene salts it has been observed that the first reduction potential is nearly constant, regardless of the position of the nitrogen atom, such a large potential difference could be ascribed, again, to the interaction in space between the aza cation and the free aza terminal, making the first reduction site less electron poor. At the same time, the reduction peak system in the −2.2/−2.8 V range looks much simpler compared to 5-aza[6]helicenium, and should correspond to reduction of the non-alkylated aza site. The azahelicenium double salt **10** features a neat couple of first reduction peaks (spaced about 0.5 V) that, considering again the above remarks about the first reduction potential of an aza cation, should be likely described as the response of two nearly equivalent redox sites, with significant reciprocal interaction along the carbohelicene chain as well as across space. This was also observed in a similar literature case [12], for which two reversible monoelectronic twin peaks are reported at −1.32 and −1.59 V. However, compared with ref. [12], in the case of **10** both reductions occur at less negative potentials, consistently with the overall more efficient conjugation. In our case, the distance between the peaks is higher, which could be ascribed to stronger reciprocal interactions. It is also worth mentioning that in cases **9** and **10**, where cation reduction results in radical formation, a possible follow-up is dimerization [12,13].

3.5. Chiral Discrimination Experiments

The three diazahelicene compounds **4**, **9** and **10** have been investigated as inherently chiral selectors by adding them in low concentration to the achiral IL 1-butyl-3-methylimidazolium bis-triflimidate [(BMIM)NTf_2] and testing the resulting three chiral media

(i) for enantioselective cyclic voltammetry experiments (CV) with the benchmark electroactive enantiomer probes (*R*)-(+)- or (*S*)-(−)- *N*,*N*′-dimethyl- 1-ferrocenylethylamine ((*R*)-Fc and (*S*)-Fc, Figure 10),

(ii) for enantioselective differential pulse voltammetry (DPV) experiments with the enantiomers of an electroactive probe of biological interest, i.e., *L*- or *D*-tryptophan (Trp), an α-amino acid (Figure 11),

both of them performed on disposable screen-printed electrode (SPE) cells on plastic polyester sheet with graphite working electrodes.

A synopsis of CV features of (*R*)-Fc and (*S*)-Fc solutions in the three tested chiral media is reported in Figure 10 (reproducibility tests are reported in Figure S7).

Enantiodiscrimination in terms of significant potential differences is observed in all cases, with the same probe enantiomer sequence (i.e., with (*R*)—undergoing easier oxidation than (*S*)-), consistently with the inherently chiral selectors **4**, **9** and **10** having the same configuration. However, the peak potential differences significantly increase from **4** to **10**, that is, with increasing number of alkylated, positively charged nitrogen atoms (**4** ~65 mV < **9** ~90 mV < **10** ~113 mV). As mentioned in the introduction, the same effect with the same probes had been observed employing as additives in achiral ionic liquids a series of compounds (non-alkylated, mono-alkylated, di-alkylated) based on an atropisomeric bipyridinium scaffold (i.e., also inherently chiral, but of axial instead of helical stereogenicity) [1].

Figures 11 and 12 account for the DPV enantioselection tests on the enantiomers of tryptophan. In particular,

- Figure 11a–c provide a comparison of the enantiodiscrimination ability of **4**, **9** and **10** as 0.02 M chiral additives in achiral commercial (BMIM)NTf_2 with L- and D-Trp (0.03 M). As in the former study case, once more the same probe enantiomer sequence (in this case,

L- before D-) is obtained with all the inherently chiral additives, but the peak potential differences significantly increase from **1** to **3** (**4** ~60 mV < **9** ~100 mV < **10** ~180 mV) that is, with increasing number of alkylated nitrogen sites.

- Figure 11d highlights the selector concentration effect in the case of inherently chiral salt **10**, the most effective selector in the series. In particular, the observed peak potential difference for the probe enantiomers is significantly larger when working with **10** at 0.02 M concentration (solid lines) with respect to 0.01 M concentration (dashed lines). A similar beneficial concentration effect has already been observed by employing as additives in achiral ionic liquids an inherently chiral molecular salt based on either an atropisomeric bipyridinium scaffold [1] or on a chiral bile acid scaffold with many stereocentres as stereogenic elements [14]. Altogether, by considering such three cases, we can assume the above concentration effect to be general.
- Testing **9** and **10** with L- and D-Trp in the 0.005–0.03 M concentration range, a linear dynamic range with very good correlation coefficients is observed for the peak currents as a function of the concentration for both enantiomers (Figure 12). Thus, quantification through peak current analysis can be added to configuration assignment based on the peak potential.

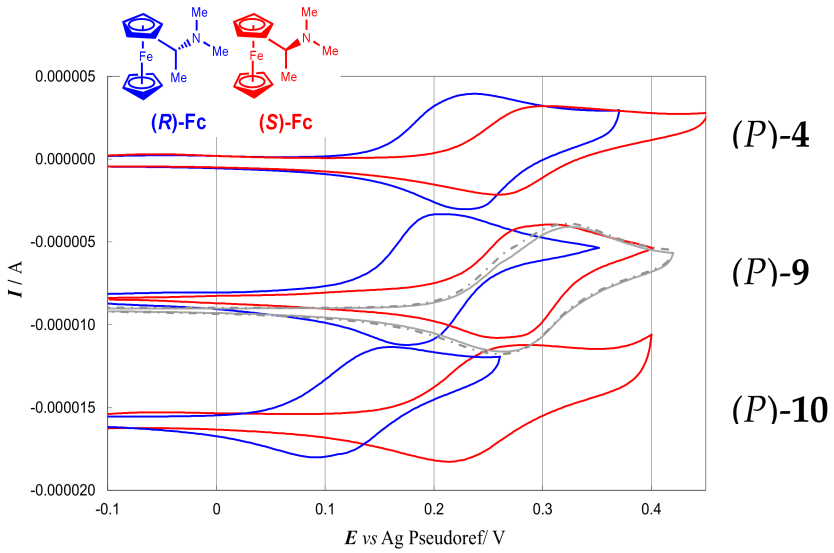

Figure 10. A synopsis of the CV features of (*R*)-Fc (blue line) and (*S*)-Fc (red line) solutions on graphite SPE in (BMIM)NTf_2 with (*P*)-**4**, (*P*)-**9** and (*P*)-**10** as low concentration chiral additives (0.02 M). In grey the voltammograms referred to experiments in absence of inherently chiral salts are also reported.

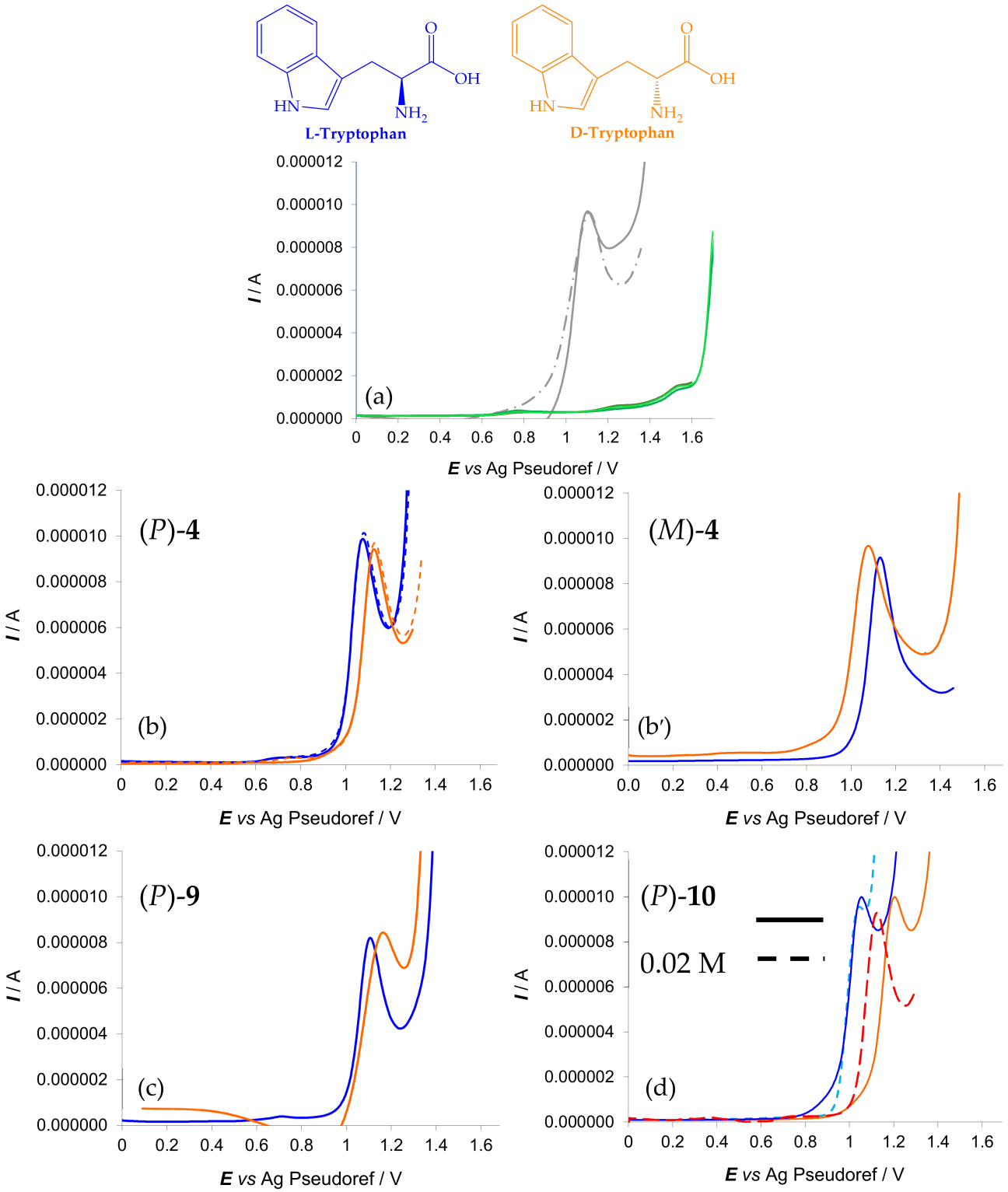

Figure 11. (**a**): DPV features of *L*- and *D*- Trp (grey dashed and straight lines respectively) in the absence of inherently chiral selectors and of (*P*)-**4**. (*P*)-**9** and (*P*)-**10** selectors in (BMIM)NTf_2 in the absence of the probes (green lines, as benchmarks). Enantioselection tests on *L*- and *D*-Trp (blue and orange, respectively) in (BMIM)NTf_2 with selectors (**b**) *(P)*-**4** 0.02 M, (**b′**) *(M)*-**4** 0.02M, (**c**) *(P)*-**9** 0.02 M and (**d**) *(P)*-**10** 0.02 M (straight lines) or 0.01 M (dashed lines).

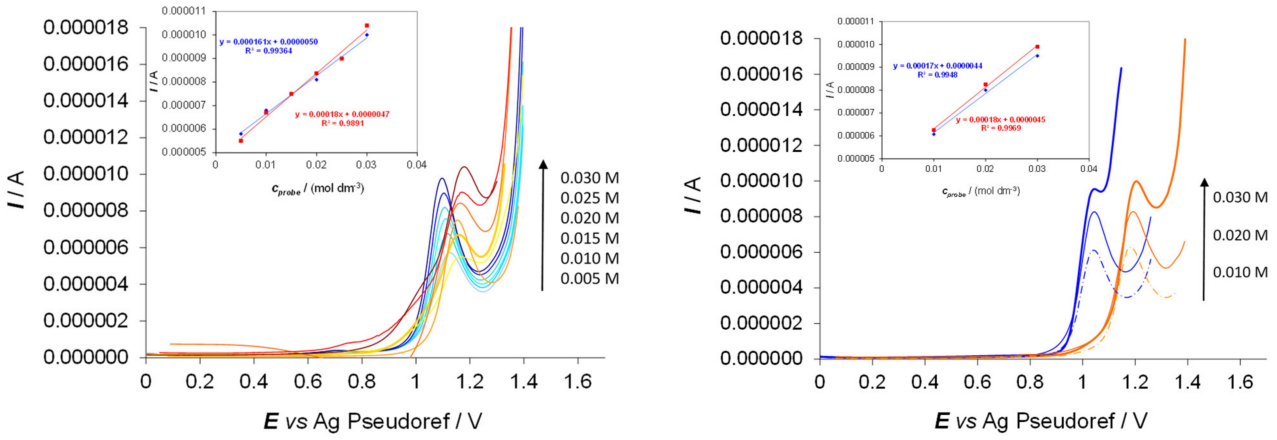

(**a**) (**b**)

Figure 12. Verification of peak current vs concentration linearity for each enantiomer. (**a**) *L*- and *D*-Trp (blue and orange lines of increasing darkness, respectively) in the 0.005–0.03 M concentration range with **2** (0.03M) in (BMIM)NTf_2. (**b**) *L*- and *D*-Trp (blue and orange, respectively) in the 0.01–0.03 M concentration range with **3** (0.03M) in (BMIM)NTf_2.

4. Conclusions

Within the framework of a research concerning inherently chiral enantiomeric selectors, 2,12-diaza[6]helicene (**4**) was synthesized and characterized. It was then converted into its *N*-mono-alkylated and *N*,*N*-di-alkylated-salts, which were used as chiral additives in commercially available achiral ionic liquids, to give media capable of distinguishing enantiomers in voltammetric experiments. Appropriate probes were selected to give preliminary information on their enantiodiscrimination ability in terms of oxidation potential differences. Outstanding peak differentiation was observed in all cases, which was more pronounced for the monoalkylated derivative than for the parent azahelicene, and even more pronounced for the doubly charged salt, in accordance with the trend previously observed for bicollidine and bibenzimidazole series, pointing to such effects being of general validity. Good linear dynamic ranges for the peak currents enable to add quantification to the configuration assignment based on peak potential.

Supplementary Materials: The following are available online at https://www.mdpi.com/article/10.3390/chemosensors9080216/s1, Figure S1: ESI mass spectrum of compound **4**, Figure S2: ^{1}H NMR of **4** (400.13 MHz, $CDCl_3$), Figure S3: APT NMR of **4** (75.47 MHz, $CDCl_3$), Figure S4: COSY plot of **4** in $CDCl_3$ (300.14 MHz), Figure S5: NOESY plot of **4** in $CDCl_3$ (300.14 MHz), Figure S6: HSQC of **4** in $CDCl_3$ (300.14 MHz), Figure S7: HMBC of (±)-**4** in $CDCl_3$ (300.14 MHz), Figure S8: ^{1}H NMR of **7** (300.14 MHz, $CDCl_3$), Figure S9: APT NMR of **7** (100.63 MHz, $CDCl_3$), Figure S10: COSY of **7** in $CDCl_3$ (300.14 MHz), Figure S11: NOESY of **7** in $CDCl_3$ (300.14 MHz), Figure S12: HSQC of **7** in $CDCl_3$ (300.14 MHz), Figure S13: ^{1}H NMR of **8** (300.14 MHz, CD_3OD), Figure S14: ^{13}C NMR of **8** (75.48 MHz, CD_3OD), Figure S15: COSY of **8** in CD_3OD (300.14 MHz, CD_3OD), Figure S16: HSQC of **8** in CD_3OD (300.14 MHz, CD_3OD), Figure S17: ^{1}H-NMR (300.14 MHz, CD_3OD), Figure S18: ^{19}F NMR (300.14 MHz, HZpPT(Hz)= 0.87, CD_3OD), Figure S19: APT NMR (100,62 MHz, CD_3OD), Figure S20: Enantioselective HPLC analysis of the enantiomers of 2,12-diaza[6]helicene isolated on a semipreparative scale, Figure S21: A synopsis of CV reproducibility checks for (*R*)-Fc (blue line) and (*S*)-Fc (red line) solutions on graphite SPE in $BMIMTf_2N$ with (*P*)-4, (*P*)-9 and (*P*)-10 as low concentration chiral additives (0.02 M).

Author Contributions: Conceptualization, F.F., S.R. and P.R.M.; formal analysis, M.T; investigation, B.B., S.G., R.C. and S.R.; resources, L.M.; writing—original draft preparation, F.F., S.R., S.G. and P.R.M.; writing—review and editing, M.T.; supervision, F.F. and P.R.M. All authors have read and agreed to the published version of the manuscript.

Funding: B.B. acknowledges funding from Università di Bergamo, Program STaRs Supporting Talented Researchers 2017–2018. P.R.M. and S.G. acknowledge financial support from the Università degli Studi di Milano. S.R. thanks Fondazione "Banca del Monte di Lombardia" for funding of the LCMS2020 mass spectrometer.

Institutional Review Board Statement: Not applicable.

Informed Consent Statement: Not applicable.

Acknowledgments: The Authors gratefully acknowledge F. Sannicolò for precious discussions as well as for kindly revising the manuscript draft and Pasquale Illiano and Donatella Nava for precious discussion on NMR characterization.

Conflicts of Interest: The authors declare no conflict of interest.

References

1. Rizzo, S.; Arnaboldi, S.; Cirilli, R.; Gennaro, A.; Isse, A.A.; Sannicolò, F.; Mussini, P.R. An "inherently chiral" 1,1′-bibenzimidazolium additive for enantioselective voltammetry in ionic liquid media. *Electrochem. Commun.* **2018**, *89*, 57–61. [CrossRef]
2. Rizzo, S.; Arnaboldi, S.; Mihali, V.; Cirilli, R.; Forni, A.; Gennaro, A.; Isse, A.A.; Pierini, M.; Mussini, P.R.; Sannicolò, F. "Inherently Chiral" Ionic-Liquid Media: Effective Chiral Electroanalysis on Achiral Electrodes. *Angew. Chem. Int. Ed.* **2017**, *56*, 2079–2082. [CrossRef] [PubMed]
3. Longhi, M.; Arnaboldi, S.; Husanu, E.; Grecchi, S.; Buzzi, I.F.; Cirilli, R.; Rizzo, S.; Chiappe, C.; Mussini, P.R.; Guazzelli, L. A family of chiral ionic liquids from the natural pool: Relationships between structure and functional properties and electrochemical enantiodiscrimination tests. *Electrochim. Acta* **2019**, *298*, 194–209. [CrossRef]
4. Bazzini, C.; Brovelli, S.; Caronna, T.; Gambarotti, C.; Giannone, M.; Macchi, P.; Meinardi, P.; Mele, A.; Panzeri, W.; Recupero, F.; et al. Synthesis and Characterization of Some Aza [5] helicenes. *Eur. J. Org. Chem.* **2005**, *2005*, 1247–1257. [CrossRef]
5. Janke, R.H.; Haufe, G.; Würthwein, E.-U.; Borkent, J.H. Racemization Barriers of Helicenes: A Computational Study. *J. Am. Chem. Soc.* **1996**, *118*, 6031–6035. [CrossRef]
6. Fontana, F.; Carminati, G.; Bertolotti, B.; Mussini, P.; Arnaboldi, S.; Grecchi, S.; Cirilli, R.; Micheli, L.; Rizzo, S. Helicity: A Non-Conventional Stereogenic Element for Designing Inherently Chiral Ionic Liquids for Electrochemical Enantiodifferentiation. *Molecules* **2021**, *26*, 311–324. [CrossRef] [PubMed]
7. Frisch, M.J.; Trucks, G.W.; Schlegel, H.B.; Scuseria, G.E.; Robb, M.A.; Cheeseman, J.R.; Scalmani, G.; Barone, V.; Mennucci, B.; Petersson, G.A.; et al. *Gaussian 09, Revision, D.01*; Gaussian, Inc.: Wallingford, CT, USA, 2013.
8. Hirshfeld, F.L. Bonded-atom fragments for describing molecular charge densities. *Theor. Chem. Acc.* **1977**, *44*, 129–138. [CrossRef]
9. Batesky, D.C.; Goldfogel, M.J.; Weix, D.J. Removal of Triphenylphosphine Oxide by Precipitation with Zinc Chloride in Polar Solvents. *J. Org. Chem.* **2017**, *82*, 9931–9936. [CrossRef] [PubMed]
10. Abbate, S.; Longhi, G.; Lebon, F.; Castiglioni, E.; Superchi, S.; Pisani, L.; Fontana, F.; Torricelli, F.; Caronna, T.; Villani, C.; et al. Helical Sense-Responsive and Substituent-Sensitive Features in Vibrational and Electronic Circular Dichroism, in Circularly Polarized Luminescence, and in Raman Spectra of Some Simple Optically Active Hexahelicenes. *J. Phys. Chem. C* **2014**, *118*, 1682–1695. [CrossRef]
11. Caronna, T.; Castiglione, F.; Famulari, A.; Fontana, F.; Malpezzi, L.; Mele, A.; Mendola, D.; Natali Sora, I. Quantum Mechanics Calculations, Basicity and Crystal Structure: The Route to Transition Metal Complexes of Azahelicenes. *Molecules* **2012**, *17*, 463–479. [CrossRef] [PubMed]
12. Brandt, J.R.; Pospisil, L.; Bednarova, L.; Correa da Costa, R.; White, A.J.P.; Mori, T.; Teply, F.; Fuchter, M.J. Intense redox-driven chiroptical switching with a 580 mV hysteresis actuated through reversible dimerization of an azoniahelicene. *Chem. Commun.* **2017**, *53*, 9059–9062. [CrossRef] [PubMed]
13. Vacek, J.; Zadny, J.; Storch, J.; Hrbac, J. Chiral Electrochemistry: Anodic Deposition of Enantiopure Helical Molecules. *ChemPlusChem* **2020**, *85*, 1954–1958. [CrossRef] [PubMed]
14. Grecchi, S.; Federghini, C.; Longhi, M.; Mezzetta, A.; Guazzelli, L.; Khawthong, S.; Arduini, F.; Chiappe, C.; Iuliano, A.; Mussini, P.R. Chiral biobased ionic liquids with cations or anions including bile acid building blocks as chiral selectors in voltammetry. *ChemElectroChem* **2021**, *8*, 1377–1387. [CrossRef]